crystals

MDPI

Article

Lattice Row Distance and Its Application in Row-Indexing

Ting Li [1,2] and Hejing Wang [1,*]

[1] School of Earth and Space Science, Peking University, Beijing 100871, China
[2] CNNC Beijing Research Institute of Uranium Geology, Beijing 100029, China; liting_c@126.com
* Correspondence: hjwang@pku.edu.cn; Tel.: +86-10-62750764

Received: 24 December 2018; Accepted: 22 January 2019; Published: 24 January 2019

Abstract: In this paper, we propose six general formulae to describe those relationships between the lattice row distance, the lattice parameters and the Miller indices h, k and l for all crystal systems along with any direction. This finally establishes the foundation of the row-indexing, a new method for deriving Miller indices from the lattice row distance. Triclinic talc is used as an example for row-indexing. This new indexing method is especially useful for beam-sensitive materials.

Keywords: formulae of lattice row distance; indexing; beam-sensitive materials; selected area electron diffraction (SAED); high resolution transmission electron microscope (HRTEM)

1. Introduction

Electron diffractometry is a powerful tool for determining crystal structure and microstructures [1]. However, there are many factors that cause "defective electron diffraction patterns" which create difficulty in structural studies and can even render these "patterns" useless. These factors include defects and local disorder in both crystal chemistry and structure [2] such as variation in thickness of the crystal [3], and fast amorphization by electron radiation damage. This phenomenon is widely found in beam-sensitive materials and "soft matter" in geology [4–6], biology [7,8], physics [9,10], inorganic chemistry [11,12] and other fields [13–16].

Li et al. [17] proposed a row-indexing method to overcome the difficulty in indexing those "defective electron diffraction patterns". However, it is only available for crystal systems other than triclinic and for those electron diffraction patterns obtained along [uv0]. According to the equation of row-row distance (X) for the monoclinic crystal system $X = [(k\boldsymbol{b}^*)^2+(h\boldsymbol{a}^*)^2(\sin\beta^*)^2]^{0.5}$ [17], the row-row distance X is a function of Miller indices h, k and lattice parameters $\boldsymbol{a}^*$, $\boldsymbol{b}^*$, β^* only, and no relation with l and $\boldsymbol{c}^*$. Therefore, the row-indexing method is useless to those electron diffraction patterns with Miler index $l \neq 0$. This limitation is also applied to cubic, tetragonal, orthorhombic, trigonal and hexagonal crystal systems [17]. In addition, it is not easy to obtain special selected-area electron diffractions (SAED) along [uv0]. The row-indexing along [uv0] is difficult to determine. Meanwhile, large amount of images of "defective electron diffraction patterns" along [uvw] are presented that contain important structural information. However, no parallel row-indexing work has been made since 2012. In this paper, we propose six formulae to describe these relationships between Miller indices h,k,l and row-row distance for all crystal systems in any orientation and finally present the foundation of "row-indexing".

2. Materials and Methods

Specimen talc (HW-1179) was collected from Shimen county, Hunan province, China. Natural talc powder was ground from the raw sample with a FD-4 hammer mill and random preparation was made for X-ray diffraction (XRD) analysis. The instrument used for XRD analysis is an X'Pert

PRO MPD (PANalytical) diffractometer with a super detector (X'Celerator). The detection parameters of the instrument were as follows: Cu Kα radiation and working at 40 kV and 40 mA, a 0.017°2θ step size, a 20 s scan time per step and a 3–70°2θ scanning range in continuous scanning mode. After measurement, software X'Pert Highscore Plus version 4.6 was used to subtract background, strip Kα2 component, search peaks and match with the diffraction pattern from ICDD 2005 [18]. Lattice parameters were refined by Unitcell after indexing. A transmission electron microscope (JEM-2100F) with energy dispersive spectrometer was used and working at 200kV to analyze lattice fringes. Sample preparation for transmission electron microscope (TEM) test was made by pipetting suspensions of ground powder onto the carbon-coated copper mesh. CrystalMaker version X was utilized for simulating the electron diffraction pattern.

3. Results

Formulae of Lattice Row Distance

Equation (1) (see Appendix A for derivation) describes the relationship between the lattice row distance (X), the Miller indices (h,k,l) and the lattice parameters ($\boldsymbol{a}^*$, $\boldsymbol{b}^*$, $\boldsymbol{c}^*$, α^*, β^*, γ^*) for the triclinic system ($a \neq b \neq c$, $\alpha \neq \beta \neq \gamma \neq 90^\circ$) along any direction.

$$X = \sqrt{\mathrm{M}/\mathrm{N}}, \tag{1}$$

where $\mathrm{M} = \mathrm{A}^2(|\boldsymbol{b}^*||\boldsymbol{c}^*|\sin\alpha^*)^2 + \mathrm{B}^2(|\boldsymbol{a}^*||\boldsymbol{b}^*|\sin\gamma^*)^2 + \mathrm{C}^2(|\boldsymbol{a}^*||\boldsymbol{c}^*|\sin\beta^*)^2 + 2\mathrm{AB}(|\boldsymbol{b}^*|^2|\boldsymbol{c}^*||\boldsymbol{a}^*|)(\sin\alpha^*\sin\gamma^*\cos\beta) + 2\mathrm{AC}(|\boldsymbol{b}^*||\boldsymbol{c}^*|^2|\boldsymbol{a}^*|)(\sin\alpha^*\sin\beta^*\cos\gamma) + 2\mathrm{BC}(|\boldsymbol{b}^*||\boldsymbol{c}^*||\boldsymbol{a}^*|^2)(\sin\beta^*\sin\gamma^*\cos\alpha)$ and $\mathrm{N} = (h_1\boldsymbol{a}^*)^2 + (k_1\boldsymbol{b}^*)^2 + (l_1\boldsymbol{c}^*)^2 + 2h_1k_1|\boldsymbol{a}^*||\boldsymbol{b}^*|\cos\gamma^* + 2k_1l_1|\boldsymbol{b}^*||\boldsymbol{c}^*|\cos\alpha^* + 2h_1l_1|\boldsymbol{a}^*||\boldsymbol{c}^*|\cos\beta^*$. Note: $\mathrm{A} = (k_2l_1 - k_1l_2)$, $\mathrm{B} = (h_2k_1 - h_1k_2)$ and $\mathrm{C} = (h_1l_2 - h_2l_1)$.

For the cubic system ($a = b = c$, $\alpha = \beta = \gamma = 90^\circ$) the formula of lattice row distance is given as:

$$X = \frac{|\boldsymbol{a}^*|\sqrt{\mathrm{A}^2 + \mathrm{B}^2 + \mathrm{C}^2}}{\sqrt{(h_1)^2 + (k_1)^2 + (l_1)^2}}, \tag{2}$$

For the tetragonal system ($a = \mathrm{b} \neq \mathrm{c}$, $\alpha = \beta = \gamma = 90^\circ$) it is given as:

$$X = \frac{|\boldsymbol{a}^*|\sqrt{\mathrm{B}^2(|\boldsymbol{a}^*|)^2 + \left[\mathrm{A}^2 + \mathrm{C}^2\right](|\boldsymbol{c}^*|)^2}}{\sqrt{(h_1 + k_1)^2(\boldsymbol{a}^*)^2 + (l_1\boldsymbol{c}^*)^2}}, \tag{3}$$

For the trigonal and hexagonal systems ($a = \mathrm{b} \neq \mathrm{c}$, $\alpha = \beta = 90^\circ$, $\gamma = 120^\circ$) given as:

$$X = \frac{|\boldsymbol{a}^*|\sqrt{\left[\mathrm{A}^2 + \mathrm{C}^2 - \mathrm{AC}\right](|\boldsymbol{c}^*|)^2 + \frac{3}{4}\mathrm{B}^2(|\boldsymbol{a}^*|)^2}}{\sqrt{[(h_1 + k_1)^2 - h_1k_1](\boldsymbol{a}^*)^2 + (l_1\boldsymbol{c}^*)^2}}, \tag{4}$$

For the orthorhombic system ($a \neq b \neq c$, $\alpha = \beta = \gamma = 90^\circ$) as:

$$X = \frac{\sqrt{\mathrm{A}^2(|\boldsymbol{b}^*||\boldsymbol{c}^*|)^2 + \mathrm{B}^2(|\boldsymbol{b}^*||\boldsymbol{a}^*|)^2 + \mathrm{C}^2(|\boldsymbol{c}^*||\boldsymbol{a}^*|)^2}}{\sqrt{[(h_1\boldsymbol{a}^*)^2 + (k_1\boldsymbol{b}^*)^2 + (l_1\boldsymbol{c}^*)^2}}, \tag{5}$$

and for the monoclinic system ($a \neq b \neq c$, $\alpha = \gamma = 90^\circ$, $\beta \neq 90^\circ$) as:

$$X = \frac{\sqrt{\mathrm{A}^2(|\boldsymbol{b}^*||\boldsymbol{c}^*|)^2 + \mathrm{B}^2(|\boldsymbol{a}^*||\boldsymbol{b}^*|)^2 + \mathrm{C}^2(|\boldsymbol{a}^*||\boldsymbol{c}^*|\sin\beta^*)^2 + \mathrm{W}}}{\sqrt{[(h_1\boldsymbol{a}^*)^2 + (k_1\boldsymbol{b}^*)^2 + (l_1\boldsymbol{c}^*)^2 + 2h_1l_1|\boldsymbol{c}^*||\boldsymbol{a}^*|\cos\beta^*}}, \tag{6}$$

where W = 2AB($|\boldsymbol{b}^*|^2 |\boldsymbol{c}^*| |\boldsymbol{a}^*|$)cosβ.

From above equations, it can be seen that Miller indices can be uniquely determined from the known lattice parameters and measured lattice row distance(s). The method of finding Miller indices from lattice row distances is termed Row-Indexing.

4. Discussion

4.1. Procedures of Row Indexing (Known Lattice Parameters)

Row-Indexing is a five-step indexing process:

(1) Measure the distance(s), X_{mea}(s), between two parallel reciprocal lattice rows in electron diffraction pattern (one of them passes through the original point). From the derivation (see Appendix A), it is clear that spot $h_1k_1l_1$ (or $h_2k_2l_2$) can represent a row and its direction (000→$h_1k_1l_1$ for instance), and that the "row distance" (000→$h_1k_1l_1$) means the perpendicular distance between this spot (and any others along the same row) and the parallel row passing through the origin. There exist many rows in many directions in a good ED pattern (Figure 1). One can measure any "row distance" in any direction. However, it should be noted that, (i) as described in Equations (1)–(6), only for a correct choice of $h_1k_1l_1$ can the X_{mea}s be (approximately) equal to the X_{cal}s; (ii) only one obvious set of rows is visible in a typical defective patterns (Figure 2a for instance), so that the number of X_{mea}(s) is small; (iii) from (ii) all rows not parallel to the actual row will produce non-matching X_{cal}s and X_{mea}(s) and will be rejected in step (3), regardless of the incident beam direction (see Table 1).

(2) Apply one of these Equations ((1)–(6), depending upon the crystal system) to the reciprocal lattice parameters and build a series of (*h*,*k*,*l*)s and corresponding X_{cal}s; Note in step (1) one can build a series of (*h*,*k*,*l*)s in the way increasing the summation of *h*,*k*,*l* and calculate their corresponding X_{cal}s.

(3) Compare X_{mea}(s) with X_{cal}s and find *h*, *k* and *l* from the closest match of X_{mea} and X_{cal}; Note that only for rows passing through this $h_1k_1l_1$ spot can X_{mea} be close to X_{cal} and the match is accepted, see Table 1 for detail.

(4) Index whole pattern based on these known *h*, *k* and *l*;

(5) Check indices according to crystallographic rules such as parallelogram law, interplanar spacing and angle formulae. Authors should discuss the results and how they can be interpreted in the perspective of previous studies and of the working hypotheses. The findings and their implications should be discussed in the broadest context possible. Future research directions may also be highlighted.

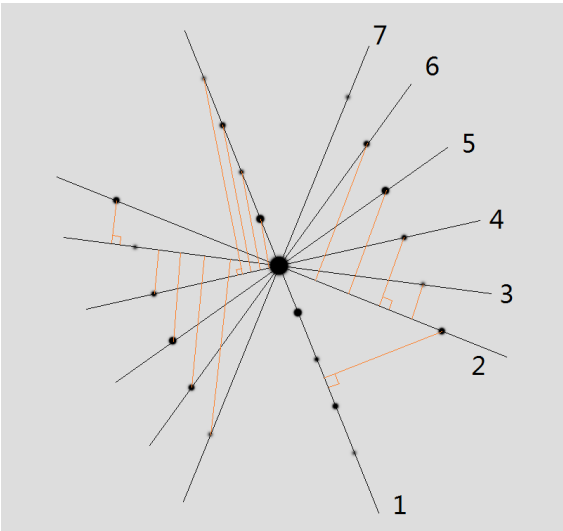

Figure 1. A good electron diffraction pattern. Numbers 1–7 mark seven lattice rows in seven different directions (black lines). Four row distances (rows 1–4) are shown as (red) lines normal to their directions.

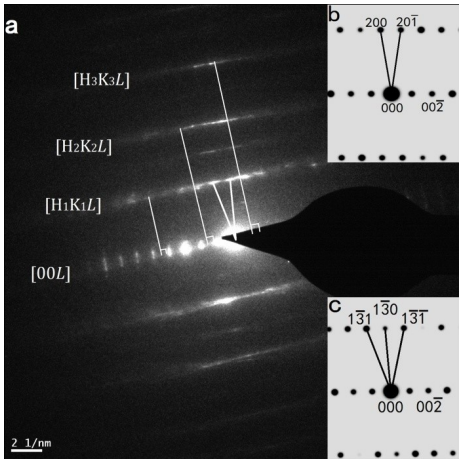

Figure 2. (**a**) Electron diffraction pattern obtained from the defective domain of talc. (**b**) The simulated electron diffraction pattern of talc incidence along [010]. (**c**) The simulated electron diffraction pattern of talc incidence along [310]. Note the angle marked by white lines in (**a**) is very similar to that in (**b**) and is noticeably different from the one in (**c**).

Table 1. Calculated and measured distances between rows and their discrepancies in electron diffraction patterns of talc (Figure 2a).

Indices			Reciprocal Space					Real Space			
h	k	l	X_{cal}	X_{mea}	X_{cal}-X_{mea}	(X_{cal}-X_{mea})/X_{cal}	$1/X_{cal}$	$1/X_{mea}$	$1/X_{cal}$-$1/X_{mea}$	($1/X_{cal}$-$1/X_{mea}$)/($1/X_{cal}$)	
0	0	1	row direction, incident along [010]								
1	3	1	0.3780	0.3796	−0.0016	0.42%	2.6455	2.6344	0.0112	0.42%	
2	6	1	0.7560	0.7593	−0.0033	0.44%	1.3227	1.3169	0.0058	0.44%	
3	9	1	1.1340	1.1286	0.0054	0.47%	0.8818	0.8861	−0.0042	0.48%	
−1	−3	1	0.3780	0.3796	−0.0016	0.42%	2.6455	2.6344	0.0112	0.42%	
−2	−6	1	0.7560	0.7593	−0.0033	0.44%	1.3227	1.3169	0.0058	0.44%	
−3	−9	1	1.1340	1.1286	0.0054	0.47%	0.8818	0.8861	−0.0042	0.47%	
−1	3	1	0.3775	0.3796	−0.0021	0.55%	2.6489	2.6344	0.0146	0.55%	ACCEPT
−2	6	1	0.7550	0.7593	−0.0043	0.57%	1.3245	1.3169	0.0075	0.56%	
−3	9	1	1.1325	1.1286	0.0039	0.35%	0.8830	0.8861	−0.0031	0.35%	
1	−3	1	0.3775	0.3796	−0.0021	0.55%	2.6489	2.6344	0.0146	0.55%	
2	−6	1	0.7550	0.7593	−0.0043	0.57%	1.3245	1.3169	0.0075	0.56%	
3	−9	1	1.1325	1.1286	0.0039	0.35%	0.8830	0.8861	−0.0031	0.35%	
±2	0	1	0.3781	0.3796	−0.0015	0.39%	2.6445	2.6344	0.0102	0.39%	
±4	0	1	0.7563	0.7593	−0.0031	0.40%	1.3223	1.3169	0.0053	0.40%	
±6	0	1	1.1344	1.1286	0.0058	0.51%	0.8815	0.8861	−0.0045	0.51%	
1	0	0	row direction, incident along [010]								
0	0	1	0.1057	0.3796	−0.2739	−259.09	9.4597	2.6344	6.8253	72.15	
2	0	2	0.2114	0.3796	−0.1682	−79.54	4.7298	2.6344	2.0955	44.30	
4	0	3	0.3171	0.3796	−0.0625	−19.70	3.1532	2.6344	0.5189	16.46	
0	0	4	0.4228	0.3796	0.0432	10.23	2.3649	2.6344	−0.2694	−11.39	
2	0	5	0.5286	0.7593	−0.2307	−43.65	1.8919	1.3170	0.5749	30.39	
−4	0	6	0.6343	0.7593	−0.1250	−19.71	1.5766	1.3170	0.2596	16.47	
1	−3	0	row direction, incident along [312]								
0	2	−1	0.1426	0.3796	−0.2370	−166.21	7.0129	2.6344	4.3786	62.44	
1	1	−2	0.2852	0.3796	−0.0944	−33.11	3.5065	2.6344	0.8721	24.87	
2	0	−3	0.4278	0.3796	0.0482	11.26	2.3376	2.6344	−0.2967	−12.69	
2	2	−4	0.5704	0.7593	−0.1889	−33.12	1.7532	1.3170	0.4362	24.88	REJECT
3	1	−5	0.7130	0.7593	−0.0463	−6.50	1.4026	1.3170	0.0856	6.10	
3	3	−6	0.8556	0.7593	0.0963	11.25	1.1688	1.3170	−0.1482	−12.68	
2	0	−3	row direction, incident along [312]								
1	1	−2	0.1172	0.3796	−0.2624	−223.88	8.5322	2.6344	5.8979	69.12	
0	−2	1	0.2344	0.3796	−0.1452	−61.94	4.2661	2.6344	1.6318	38.25	
1	−3	0	0.3516	0.3796	−0.0280	−7.96	2.8441	2.6344	0.2097	7.37	
0	−4	2	0.4688	0.3796	0.0892	19.03	2.1331	2.6344	−0.5013	−23.50	
1	−5	1	0.5860	0.7593	−0.1733	−29.57	1.7064	1.3170	0.3894	22.82	
2	−6	0	0.7032	0.7593	−0.0561	−7.98	1.4220	1.3170	0.1050	7.39	
1	−1	−1	row direction, incident along [312]								
0	2	−1	0.2327	0.3796	−0.1469	−63.16	4.2983	2.6344	1.6639	38.71	
1	3	−3	0.4653	0.3796	0.0857	18.42	2.1491	2.6344	−0.4852	−22.58	
2	4	−5	0.6980	0.7593	−0.0613	−8.79	1.4328	1.3170	0.1158	8.08	
2	6	−6	0.9306	1.1286	−0.1980	−21.28	1.0746	0.8861	0.1885	17.54	

Note: subscripts mea and cal stand for the measured and the calculated respectively and the unit of $1/X_{mea}$ and $1/X_{cal}$ is Å.

4.2. Validating By Electron Diffraction Patterns

Clay minerals are typical beam-sensitive materials and develop abundant defects and dislocations in their structures. Such defects and dislocations in structure and their beam-sensitive properties easily result in defective SAED patterns and cause considerable difficulty for indexing. "Row-Indexing" can effectively overcome these difficulties.

Talc ($Mg_3(Si_2O_5)_2(OH)_2$) from Hunan province, south China is used for high resolution transmission electron microscope (HRTEM) analysis. Its lattice parameters are obtained from powder X-ray diffraction as a = 5.2891 Å, b = 9.1735 Å, c = 9.4600 Å, α = 90.460°, β = 98.683°, γ = 90.085°. Orientation technique [17] is performed to provide a [uv0] sample that contains the most important structure information [5]. Following Section 4.1, these procedures of row-indexing for SAED patterns of talc are given below.

Step 1: Measure the distances X_{mea}s between [00L] and [HnKnL] (we use capital letters H, K and L with [ ] to represent reciprocal lattice row(s) to distinguish from the Miller indices h, k and l) in SAED patterns of talc (Figure 2a). Step 2: Compare them with a series of X_{cal}s calculated by Equation (1). Step 3: Find out that those with the least difference between X_{mea} and X_{cal} are from the incident direction [010]/[0$\bar{1}$0] or [310]/[3$\bar{1}$0]/[$\bar{3}$10]/[$\bar{3}\bar{1}$0]. Steps 4–5: Determine the right incidence direction ([010]/[0$\bar{1}$0]) from the position of diffraction spots near the origin (Figure 2b,c) and obtain the correct Miller indices (see Table 1).

The row-indexing is also verified by published data (see Table 2).

Table 2. Calculated and measured distances between rows and their discrepancies in electron diffraction patterns of ZnPc [16] and Octacalcium phosphate (OCP) [19].

Indices			Reciprocal Space						Real Space		
h	k	l	X_{cal}	X_{mea}	X_{cal}-X_{mea}	(X_{cal}-X_{mea})/X_{cal}	$1/X_{cal}$	$1/X_{mea}$	$1/X_{cal}$-$1/X_{mea}$	($1/X_{cal}$-$1/X_{mea}$)/($1/X_{cal}$)	
h	h	l	row direction, incident along [110], ZnPc (figure-3c in [16])								
−2	2	0	0.214	0.217	−0.0026	−1.21%	4.673	4.617	0.056	1.20%	
0	0	4	0.585	0.582	0.0035	0.60%	1.709	1.720	−0.010	−0.60%	
−2	2	2	0.361	0.359	0.002	0.55%	2.770	2.786	−0.015	−0.56%	
−2	2	−1	0.26	0.263	−0.003	−1.15%	3.846	3.802	0.044	1.14%	
−2	2	1	0.258	0.254	0.004	1.55%	3.876	3.937	−0.061	−1.57%	ACCEPT
−2	2	−4	0.624	0.629	−0.005	−0.80%	1.603	1.590	0.013	0.79%	
3	−3	3	0.545	0.559	−0.014	−2.57%	1.835	1.789	0.046	2.50%	
3	−3	−4	0.665	0.676	−0.011	−1.65%	1.504	1.479	0.024	1.63%	
−6	6	4	0.864	0.889	−0.025	−2.89%	1.157	1.125	0.033	2.81%	
h	h	l	row direction, incident along [110], OCP (figure-6f in [19])								
0	0	4	0.16523	0.16545	−0.00022	−0.13%	6.052	6.044	0.008	0.13%	
1	−1	3	0.295	0.297	−0.002	−0.68%	3.390	3.367	0.023	0.67%	
1	−1	−3	0.294	0.3	−0.006	−2.04%	3.401	3.333	0.068	2.00%	
−1	1	3	0.294	0.302	−0.008	−2.72%	3.401	3.311	0.090	2.65%	
1	−1	2	0.28	0.2804	−0.0004	−0.14%	3.571	3.566	0.005	0.14%	
−1	1	2	0.28	0.281	−0.001	−0.36%	3.571	3.559	0.013	0.36%	
−1	1	4	0.314	0.321	−0.007	−2.23%	3.185	3.115	0.069	2.18%	
1	−1	4	0.314	0.316	−0.002	−0.64%	3.185	3.165	0.020	0.63%	
1	−1	−4	0.314	0.321	−0.007	−2.23%	3.185	3.115	0.069	2.18%	
0	0	−6	0.248	0.256	−0.008	−3.23%	4.032	3.906	0.126	3.13%	*
0	0	−12	0.496	0.518	−0.022	−4.44%	2.016	1.931	0.086	4.25%	*
1	−1	−4	0.314	0.312	0.002	0.64%	3.185	3.205	−0.020	−0.64%	**

Note: subscripts mea and cal stand for the measured and the calculated respectively and the unit of $1/X_{mea}$ and $1/X_{cal}$ is Å. *: reject (err >3%), **: reject (spot not on row).

5. Conclusions

Lattice row distance describes the distance from a row to the origin in reciprocal space. Any electron diffraction pattern consists of many but limited groups of rows in different orientation. A group of rows comprises a series of parallel rows in the same orientation and in a special interval of lattice row distance. The weakness, deformation and tailing of diffraction spots produced from beam-sensitive materials and "soft matter" make rows clear and outstanding.

The proposed equations well describe the relationships between the lattice row distances, the Miller indices and the reciprocal lattice parameters. Clear rows allow row-indexing to overcome the

difficulties caused by spot weakness and deformation and make it possible to index those defective or weak electron diffraction patterns. The Row-indexing can be also applied to the FFT of HRTEM images.

Author Contributions: Conceptualization, W.H.J. and L.T.; methodology, L.T.; software, W.H.J.; validation, L.T., and W.H.J.; formal analysis, L.T.; investigation, L.T.; resources, W.H.J.; data curation, L.T.; writing—original draft preparation, L.T.; writing—review and editing, W.H.J.; supervision, W.H.J.; project administration, W.H.J.; funding acquisition, W.H.J.

Funding: This research was funded by The National Natural Science Foundation of China, grant number 41872048, 40972038, 40872034.

Acknowledgments: We are grateful to Fan, H.H. at school of mathematical sciences and Yu, D.P. at school of physics, Peking University for their constructional suggestions on the formula deduction of the triclinic system.

Conflicts of Interest: The authors declare no conflict of interest. The funders had no role in the design of the study; in the collection, analyses, or interpretation of data; in the writing of the manuscript, or in the decision to publish the results.

Appendix A. Derivation of Lattice Row Distance Formulae

From the geometric relation of seven crystal systems, it is easy to understand that transforming from the triclinic to one of the other six crystal systems requires imposing specific geometric conditions on the lattice parameters. Therefore, a general formula describing the relationship between the lattice row distance, the Miller index h, k, and l and the lattice parameters for the triclinic system along all incident directions would be the solution for all crystal systems.

For the triclinic system, $a \neq b \neq c$, $\alpha \neq \beta \neq \gamma$; $\boldsymbol{ab}^* = \boldsymbol{ac}^* = \boldsymbol{ba}^* = \boldsymbol{bc}^* = \boldsymbol{ca}^* = \boldsymbol{cb}^* = 0$; $\boldsymbol{a}^* = (\boldsymbol{b} \times \boldsymbol{c})/\mathrm{V}$; $\boldsymbol{b}^* = (\boldsymbol{a} \times \boldsymbol{c})/\mathrm{V}$; $\boldsymbol{c}^* = (\boldsymbol{a} \times \boldsymbol{b})/\mathrm{V}$; $\alpha^* = \cos^{-1}[(\cos\beta\cos\gamma\text{-}\cos\alpha)/(\sin\beta\sin\gamma)]$; $\beta^* = \cos^{-1}[(\cos\alpha\cos\gamma\text{-}\cos\beta)/(\sin\alpha\sin\gamma)]$; $\gamma^* = \cos^{-1}[(\cos\alpha\cos\beta\text{-}\cos\gamma)/(\sin\alpha\sin\beta)]$. Note $\times$ denotes the vector cross product.

Suppose (Figure A1) that O is the origin (000); A ($h_1k_1l_1$) and B ($h_2k_2l_2$) are two lattice points and **OA** ($h_1\boldsymbol{a}^*$, $k_1\boldsymbol{b}^*$, $l_1\boldsymbol{c}^*$) and **OB** ($h_2\boldsymbol{a}^*$, $k_2\boldsymbol{b}^*$, $l_2\boldsymbol{c}^*$) are their vectors; X is the distance between B and lattice row OA in reciprocal space (note that X is also the perpendicular distance between any pair of lattice rows parallel to OA). The dashed region denotes the triangle ΔOAB, and its area ($S_{\Delta OAB}$) is equal to half the product of the magnitude of **OA** multiplied by X or equal to half the area of the parallelogram that vectors **OA** and **OB** span.

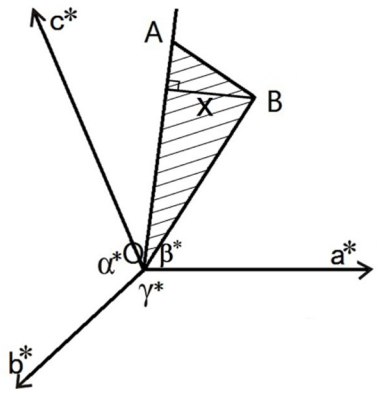

Figure A1. Reciprocal lattice of the triclinic system.

According to the definition, the magnitude (signed as | |) of vector cross product is equal to the area of the parallelogram spanned by two vectors. Thus,

$$S\Delta_{\mathrm{OAB}} = 0.5|\mathbf{OA} \times \mathbf{OB}| = 0.5|(h_1\boldsymbol{a}^*, k_1\boldsymbol{b}^*, l_1\boldsymbol{c}^*) \times (h_2\boldsymbol{a}^*, k_2\boldsymbol{b}^*, l_2\boldsymbol{c}^*)| = 0.5|h_1h_2(\boldsymbol{a}^* \times \boldsymbol{a}^*) + h_1k_2(\boldsymbol{a}^* \times \boldsymbol{b}^*) + h_1l_2(\boldsymbol{a}^* \times \boldsymbol{c}^*) + k_1h_2(\boldsymbol{b}^* \times \boldsymbol{a}^*) + k_1k_2(\boldsymbol{b}^* \times \boldsymbol{b}^*) + k_1l_2(\boldsymbol{b}^* \times \boldsymbol{c}^*) + l_1h_2(\boldsymbol{c}^* \times \boldsymbol{a}^*) + l_1k_2(\boldsymbol{c}^* \times \boldsymbol{b}^*) + l_1l_2(textbfc^* \times \boldsymbol{c}^*)|, \quad \text{(A1)}$$

In a right-handed coordinate system we have
$\boldsymbol{a}^* \times \boldsymbol{a}^* = 0$, $\boldsymbol{b}^* \times \boldsymbol{b}^* = 0$, $\boldsymbol{c}^* \times \boldsymbol{c}^* = 0$, $\boldsymbol{b}^* \times \boldsymbol{a}^* = -(\boldsymbol{a}^* \times \boldsymbol{b}^*)$, $\boldsymbol{c}^* \times \boldsymbol{b}^* = -(\boldsymbol{b}^* \times \boldsymbol{c}^*)$ and $\boldsymbol{a}^* \times \boldsymbol{c}^* = -(\boldsymbol{c}^* \times \boldsymbol{a}^*)$.
Hence, $S_{\Delta OAB}$ can be expressed as

$$S_{\Delta OAB} = 0.5\,|\,A(\boldsymbol{c}^* \times \boldsymbol{b}^*), C(\boldsymbol{a}^* \times \boldsymbol{c}^*), B(\boldsymbol{b}^* \times \boldsymbol{a}^*)\,|\,, \tag{A2}$$

Note: $A = (k_2l_1 - k_1l_2)$, $B = (h_2k_1 - h_1k_2)$ and $C = (h_1l_2 - h_2l_1)$.
According to the definition of vector dot product (signed as •), for example $|\,\boldsymbol{a}\,| = (\boldsymbol{a} \bullet \boldsymbol{a})^{1/2}$ [20], we have

$$|\,A(\boldsymbol{c}^* \times \boldsymbol{b}^*), C(\boldsymbol{a}^* \times \boldsymbol{c}^*), B(\boldsymbol{b}^* \times \boldsymbol{a}^*)\,| = \{[A(\boldsymbol{c}^* \times \boldsymbol{b}^*), C(\boldsymbol{a}^* \times \boldsymbol{c}^*), B(\boldsymbol{b}^* \times \boldsymbol{a}^*)] \bullet [A(\boldsymbol{c}^* \times \boldsymbol{b}^*), C(\boldsymbol{a}^* \times \boldsymbol{c}^*), B(\boldsymbol{b}^* \times \boldsymbol{a}^*)]\}^{1/2}, \tag{A3}$$

Therefore,

$$\begin{aligned} S_{\Delta OAB} = 0.5[&A^2(|\,\boldsymbol{b}^*\,|\,|\,\boldsymbol{c}^*\,|\sin\alpha^*)^2 + B^2(|\,\boldsymbol{a}^*\,|\,|\,\boldsymbol{b}^*\,|\sin\gamma^*)^2 + C^2(|\,\boldsymbol{a}^*\,|\,|\,\boldsymbol{c}^*\,|\sin\beta^*)^2 \\ &+ 2AB\,|\,\boldsymbol{b}^*\,|^2\,|\,\boldsymbol{c}^*\,|\,|\,\boldsymbol{a}^*\,|\sin\alpha^*\sin\gamma^*\cos\beta + 2AC\,|\,\boldsymbol{b}^*\,|\,|\,\boldsymbol{c}^*\,|^2\,|\,\boldsymbol{a}^*\,|\sin\alpha^*\sin\beta^*\cos\gamma \\ &+ 2BC\,|\,\boldsymbol{b}^*\,|\,|\,\boldsymbol{c}^*\,|\,|\,\boldsymbol{a}^*\,|^2\sin\beta^*\sin\gamma^*\cos\alpha]^{0.5} \end{aligned} \tag{A4}$$

From the interplanar spacing formula of the triclinic system, $|\,OA\,|$ is given as

$$|\,OA\,| = [(h_1\boldsymbol{a}^*)^2 + (k_1\boldsymbol{b}^*)^2 + (l_1\boldsymbol{c}^*)^2 + 2h_1k_1\,|\,\boldsymbol{a}^*\,|\,|\,\boldsymbol{b}^*\,|\cos\gamma^* + 2k_1l_1\,|\,\boldsymbol{b}^*\,|\,|\,\boldsymbol{c}^*\,|\cos\alpha^* + 2h_1l_1\,|\,\boldsymbol{a}^*\,|\,|\,\boldsymbol{c}^*\,|\cos\beta^*]^{0.5} \tag{A5}$$

Based on Equations (A4) and (A5) and $S_{\Delta OAB} = 0.5|OA|X$, the X is finally written as Equation (1). All other equations for other crystal systems can be derived from Equation (1) and are given as Equations (2)–(6).

References

1. Cowley, J.W. Electron diffraction: An introduction. In *Electron Diffraction Techniques*; Cowley, J.M., Ed.; Oxford University Press: London, UK, 1992; pp. 1–75.
2. Daisuke, S.; Kenji, H. (Eds.) *High-Resolution Electron Microscopy for Materials Science*; Springer: Tokyo, Japan, 1998; pp. 41–82. [CrossRef]
3. Plancon, A. New modeling of X-ray diffraction by disordered lamellar structures, such as phyllosilicates. *Am. Miner.* **2002**, *87*, 1672–1677. [CrossRef]
4. Chen, T.; Wang, H.J.; Zhang, X.P.; Zheng, N. SAED and HRTEM investigation of palygorskite. *Acta Geol. Sin.* **2008**, *82*, 385–391. [CrossRef]
5. Kogure, T. Investigations of micas using advanced transmission electron microscopy. *Rev. Miner. Geochem.* **2002**, *46*, 281–312. [CrossRef]
6. Schmidt, D.; Livi, K.J.T. HRTEM and SAED investigations of polytypism, stacking disorder, crystal growth, and vacancies in chlorites from subgreenschist facies outcrops. *Am. Miner.* **1999**, *84*, 160–170. [CrossRef]
7. Jee, S.S.; Culver, L.; Li, Y.; Douglas, E.P.; Gower, L.B. Biomimetic mineralization of collagen via an enzyme-aided PILP process. *J. Cryst. Growth* **2010**, *312*, 1249–1256. [CrossRef]
8. Wang, H.J.; Yuan, L.; An, J.L. Crystallographic Characteristics of Hydroxylapatite in Hard Tissues of Cololabis Saira. *Crystals* **2017**, *7*, 103. [CrossRef]
9. Yoon, S.M.; Hwang, I.C.; Shin, N.; Ahn, D.; Lee, S.J.; Lee, J.Y.; Choi, H.C. Vaporization-condensation-recrystallization process-mediated synthesis of helical m-aminobenzoic acid nanobelts. *Langmuir* **2007**, *23*, 11875–11882. [CrossRef] [PubMed]
10. Wang, Y.Q.; Duan, X.F. Crystalline boron nanowires. *Appl. Phys. Lett.* **2003**, *82*, 272–274. [CrossRef]
11. Zhang, S.; Yuan, G.Y.; Lu, C.; Ding, W.J. The relationship between $(Mg, Zn)_3RE$ phase and 14H-LPSO phase in Mg–Gd–Y–Zn–Zr alloys solidified at different cooling rates. *J. Alloy. Compd.* **2011**, *509*, 3515–3521. [CrossRef]
12. Olafsen, A.; Larsson, A.K.; Fjellvasg, H.; Hauback, B.C. On the Crystal Structure of $Ln_2O_2CO_3$ II (Ln = La and Nd). *J. Solid State Chem.* **2001**, *158*, 14–24. [CrossRef]

13. Matsushita, I.; Hamada, Y.; Suzuki, T.; Nomura, Y.; Moriga, T.; Ashida, T.; Nakabayashi, I. Crystal-structure of basic calcium-carbonate and its decomposition process in water. *J. Ceram. Soc. Jpn.* **1993**, *101*, 1335–1339. [CrossRef]
14. Weng, X.; Li, C.Y.; Jin, S.; Zhang, D.; Zhang, J.Z.; Bai, F.; Harris, F.W.; Cheng, S.Z.D.; Lotz, B. Helical Twist Senses, Liquid Crystalline Behavior, Crystal Microtwins, and Rotation Twins in a Polyester Containing Main-Chain Molecular Asymmetry and Effects of the Number of Methylene Units in the Backbones on the Phase Structures and Morphologies of Its Homologues. *Macromolecules* **2002**, *35*, 9678–9686. [CrossRef]
15. Siddaramanna, A.; Thipperudraiah, K.V.; Chandrappa, G.T. Simple non-basic solution route for the preparation of zinc oxide hollow spheres. *Phys. E Low-Dimens. Sys. Nanostru.* **2012**, *44*, 1346–1350. [CrossRef]
16. Qiao, X.; Chang, H.; Huang, L.; Zhang, J.; Tian, H.; Geng, Y.; Yan, D. Highly ordered thin films of 5,5″-bis(3′-fluoro-biphenyl-4-yl)-2,2′:5′,2″-terthiophene with two meso-phases. *Phys. Chem. Chem. Phys.* **2012**, *14*, 10279–10284. [CrossRef] [PubMed]
17. Li, T.; Wang, H.J.; Fan, E.P.; Wang, L.; Zhou, Z. "Row Indexing" of electron diffraction patterns along [uv0]. *Z. Kristallogr.* **2012**, *227*, 665–671. [CrossRef]
18. International Centre of Diffraction Database (ICDD). version 2005.
19. Arellano-Jiménez, M.J.; García-García, R.; Reyes-Gasga, J. Synthesis and hydrolysis of octacalcium phosphate and its characterization by electron microscopy and X-ray diffraction. *J. Phys. Chem. Solids* **2009**, *70*, 390–395. [CrossRef]
20. Gao, H.Z.; Wang, J.G.; Fu, R.N. *Space Analytic Geometry*; Beijing Normal University Press: Beijing, China, 2007; p. 40. (In Chinese)